NREL/TP-451-21584 • UC Category: 1262 • DE96013075

Microstructure of Amorphous-Silicon-Based Solar Cell Materials by Small-Angle X-Ray Scattering

Annual Technical Report, 6 April 1995 - 5 April 1996

D.L. Williamson
Department of Physics
Colorado School of Mines
Golden, Colorado

NREL technical monitor: B. von Roedern

National Renewable Energy Laboratory
1617 Cole Boulevard
Golden, Colorado 80401-3393
A national laboratory of
the U.S. Department of Energy
Managed by Midwest Research Institute
for the U.S. Department of Energy
under Contract No. DE-AC36-83CH10093

Prepared under Subcontract No. XAN-4-13318-04

August 1996

NOTICE

Available to DOE and DOE contractors from:
Office of Scientific and Technical Information (OSTI)
P.O. Box 62
Oak Ridge, TN 37831
Prices available by calling (423) 576-8401

Available to the public from:
National Technical Information Service (NTIS)
U.S. Department of Commerce
5285 Port Royal Road
Springfield, VA 22161
(703) 487-4650

Printed on paper containing at least 50% wastepaper, including 10% postconsumer waste

TABLE OF CONTENTS

page

LIST OF FIGURES

page

LIST OF TABLES

1. EXECUTIVE SUMMARY

1.1 PREFACE

This report presents results of research performed from April 6, 1995 to April 5, 1996 under a cost-reimbursible subcontract from the National Renewable Energy Laboratory (NREL, a national laboratory of the U.S. Department of Energy operated by Midwest Research Institute) to the Colorado School of Mines (subcontract number XAN-4-13318-04 to the prime contract DE-AC02-83CH10093). The research was carried out under the direction of Don L. Williamson, Professor of Physics. Materials characterization, including small-angle x-ray scattering, x-ray diffraction, and flotation density, were carried out in the Physics Department of the Colorado School of Mines. The materials for analyses were supplied by NREL-supported device-making groups as well as by other groups with relevant expertise. Electron microprobe analyses of film compositions were carried out by Alice Mason of NREL. TEM measurements were made by Kim Jones of NREL. Graduate research assistant Steve Johnston participated in all aspects of the research in pursuit of his Ph.D. degree in Materials Science.

1.2 OBJECTIVES

The general objective of this research is to provide detailed microstructural information on the amorphous-silicon-based, thin-film materials under development for improved multijunction solar cells. Correlation of this microstructure with opto-electronic properties and device performance is an integral part of the research. The experimental technique used is small-angle x-ray scattering (SAXS) and it provides quantitative microstructural data on microvoid fractions, sizes, shapes, and their preferred orientations. Other microstructural features such as alloy segregation, hydrogen-rich clusters and alloy short-range order are probed. Three types of material are under investigation and fall into the bandgap classification scheme forming the basis of three of the four NREL Amorphous Silicon Teams. Specific projects in each of the Team areas that were addressed during this second phase are listed below, followed by the principal conclusions from each project.

1.2.1 Low-bandgap Materials

a. Complete the analysis of the Harvard Ge-rich a-$Si_{1-x}Ge_x$:H films prepared on the powered electrode of a PECVD system and make correlation with opto-electronic properties.

b. Examine USSC a-$Si_{1-x}Ge_x$:H material prepared at high deposition rates by microwave

plasma technique.

c. Study IACS a-Si:H low-bandgap films prepared by He dilution of silane plasma.

d. Continue application of ASAXS method to search for evidence of Ge composition fluctuations in a-$Si_{1-x}Ge_x$:H films prepared by several groups.

1.2.2 Mid-bandgap Materials

a. Examine the hotwire CVD a-Si:H presently being tested in devices by NREL/USSC.

b. Characterize the ECD a-Si:H material used to make their single-junction cells with V_{oc} >1 volt.

c. Investigate the effect of p-type doping on the nanostructure of a-Si:H prepared by PECVD.

1.2.3 High-bandgap Materials

a. Study the high-bandgap a-Si:H material prepared at TIT by the chemical annealing technique.

1.3 CONCLUSIONS

1.3.1 Low-bandgap Materials

a. PECVD a-$Si_{1-x}Ge_x$:H films deposited on the cathode of an rf discharge possess opto-electronic properties that are greatly improved over any yet reported in the range of $x \geq 0.6$. The improvements are attributed in large part to the reduction in structural inhomogeneity as observed by SAXS, and partly to a reduction in midgap state density. The conditions of deposition that lead to these improvements are believed to be high electron temperature in the discharge plasma, which leads to favorable chemical radicals and high levels of ion bombardment.

b. It is possible to produce a-$Si_{1-x}Ge_x$:H films via the microwave plasma technique at a deposition rate of 4 nm/s with no detectable nanostructure and a void fraction below 0.01 vol.%. The formation of these structurally homogeneous materials is critically dependent on the application of a substrate bias during deposition. The material made under the bias on condition yields the better solar cells.

c. The He-diluted silane films of a-Si:H are nanostructurally homogeneous such that void fractions are below the detection limit of 0.01 vol.%. Some larger-scale features are present that may be due to residual columnar-like microstructure. This material has optical (Tauc) bandgaps as low as 1.50 eV with $\eta\mu\tau=6x10^{-5}$ cm^2/V. Attempts to produce similar material at USSC were not successful in that lower V_{oc} devices could not be fabricated.

d. Analysis of ASAXS data obtained at the German synchrotron facility (DESY) provides evidence of a non-uniform Ge distribution in one a-$Si_{1-x}Ge_x$:H film prepared at IACS. The Ge composition fluctuations mimic the columnar-like microstructure previously reported for this material, suggesting that the Ge may be clustering along the column boundaries.

1.3.2 Mid-bandgap Materials

a. A film of hotwire a-Si:H, prepared with the same conditions presently being used to make solar cells in a team project involving NREL and USSC, has no detectable nanostructure and a void fraction below the detection limit of 0.01 vol.%. This film also has the highest flotation density (2.292 g/cm^3) and a diffuse SAXS signal lower than any previous a-Si:H film, consistent with the lower H content (2-3 at.%) in this material.

b. An a-Si:H film deposited under conditions that yield single-junction cells with initial V_{OC} = 1.04-1.05 V and stabilized V_{OC} = 1.01 V at ECD shows no detectable nanostructure and a void density well below 0.1 vol.%. This is of interest since the low deposition temperature of 150°C leads to a high H content (estimated at ~18 at. % based on the measured flotation density, 2.166 g/cm^3, and the diffuse SAXS signal). The use of high H_2 dilution seems to promote the homogeneous nanostructure.

c. Doping of a-Si:H with B via a 1% TMB-in-He source during PECVD deposition leads to a dramatic increase in 1 nm-sized nanostructure that increases systematically with the amount of doping. Assuming nanovoids, their volume fraction reaches 2.1 vol.%, a factor of about 50 larger than the undoped material.

1.3.3 High-bandgap Materials

a. Two sets of a-Si:H films prepared at TIT by the chemical annealing technique at low substrate temperatures (50-125°C) have high H contents and high optical bandgaps (1.91-2.05 eV). Some of the samples were partially microcrystalline but those that remained fully amorphous had significant inhomogeneity as detected by SAXS. Low flotation densities are consistent with high H contents and the presence of microvoids, sometimes at the 1 vol.% level. The opto-electronic behavior of this type of material suggests device-quality properties and enhanced stability but its use in a device has not been tested to our knowledge.

2. INTRODUCTION

During this second phase of our three-year program we have obtained information on the microstructure of materials relevant to the Low-, Mid-, and High-bandgap Teams and the results are appropriately divided into these three types of material as presented below. The experimental methods, data analysis, and interpretation procedures are the same as those described in detail in the phase-one report [1] and in the review paper published last year [2]. Samples have been supplied by the following Team members for SAXS projects: P. Wickboldt, Harvard University (now at Lawrence Livermore National Laboratory); S. Guha, USSC; H. Mahan, NREL; S. Jones, ECD. In addition, samples have been supplied by other groups working on a-Si-based solar cell materials and are relevant to our Team efforts: S. Ray, IACS; G. Moddel, University of Colorado at Boulder (UCB), I. Shimizu, Tokyo Institute of Technology (TIT).

3. LOW-BANDGAP MATERIALS

3.1 Harvard Ge-Rich Alloys (a-$Si_{1-x}Ge_x$:H)

Figure 1 and Table 1 display the results of the SAXS measurements on 9 cathodic (powered electrode) a-$Si_{1-x}Ge_x$:H alloys and one anodic sample with x=1 which have been separated into two groups: those made using conditions which yield films with poorer opto-electronic properties (non-optimized); and those related to superior opto-electronic properties (optimized). Note that for the two x=1 samples the SAXS is much stronger for the anodic film. However, the integrated signal (Q) from the cathodic x=1 film is still much larger than that from a-Si:H (NREL sample data is included in Table 1).

To demonstrate the improved opto-electronic properties of the cathodic alloys, Fig. 2 compares the $\eta\mu\tau$ of a set of optimized alloys with those from a set of previously studied anodic alloys [3]. There is a remarkable improvement for E_{04} below 1.6 eV, corresponding to $x \geq 0.6$. Other properties showing improvements include ambipolar diffusion lengths, midgap state densities, Urbach tail widths, and photoluminescence.

Returning to the SAXS alloy data in Fig.1 and Table 1, note the much reduced integrated intensity for the optimized alloys, supporting the thesis that removing structural heterogeneity will improve opto-electronic properties. For half the optimized alloys, Q, and the calculated void fraction, f, are below the detection limit, implying structural homogeneity comparable to device quality a-Si:H. The correlation between structure and electronic properties has some limits; within the set of optimized alloys, there is not a one-to-one relation between either Q or f and the opto-electronic properties of films identically prepared. This does not imply that the remaining small degree of heterogeneity does not have an effect on the opto-electronic properties, only that any such effect is not

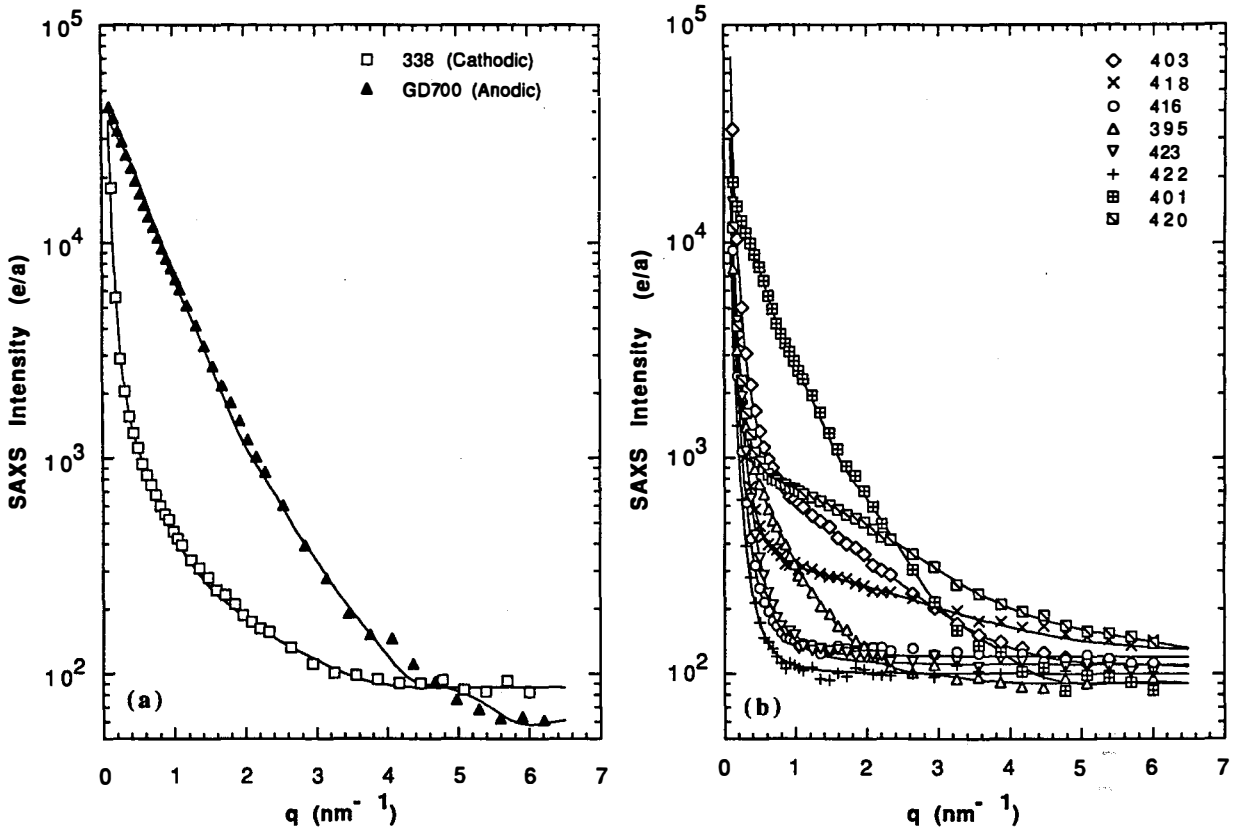

Fig. 1. SAXS intensity from Harvard films: (a) anodic and cathodic a-Ge:H (b) 8 cathodic a-$Si_{1-x}Ge_x$:H alloys.

Table 1. SAXS results from Harvard Ge-rich a-$Si_{1-x}Ge_x$:H alloys.

Sample	x	Comments	Q (10^{24} eu·cm^{-3})	I_d (eu)	f (%)	Q_0/Q_{45}	⟨R⟩ (nm)
GD 700	1.00	Anodic a-Ge:H	31.0	50	3.9	5.2	2.0
338	1.00	Standard Cathodic a-Ge:H	1.8	85	0.22	5.1	1.6
403	0.86	Optimized	3.5	105	0.50	2.6	1.0
418	0.76	Optimized	2.15	128	0.34	1.6	0.7
416	0.74	Optimized	<0.2[a]	120	<0.03	b	---
395	0.72	Optimized	1.0	90	0.16	>1[c]	2.0
423	0.70	Optimized	<0.2[a]	110	<0.03	b	---
422	0.69	Optimized	<0.2[a]	100	<0.03	b	---
401	0.84	Non-optimized	13.7	85	2.01	~5[c]	2.0
420	0.75	Non-optimized	6.5	115	1.05	2.1	0.7
NREL 71i	0	Device-quality a-Si:H	<0.02[a]	7	<0.01	b	3.8

a. Estimated lower detection limit
b. Unable to determine due to weak I_N signals.
c. Less than usual accuracy due to thin samples.

dominant.

For samples with sufficient signal to determine Q_0/Q_{45}, all the values are well above unity. Thus much of the remaining heterogeneity in the cathodic alloys is probably caused by residual columnar-like growth. For the full set of samples measured, the average void size varies from 0.7 nm to 2.0 nm with no apparent trend. The diffuse scattering, I_d, is higher in the alloys than in the standard cathodic a-Ge:H. This is accounted for by the increased Laue scattering due to both the Si alloying and the increased H content [1].

A paper describing all the opto-electronic results and the correlation with the SAXS for this set of alloys has been submitted to J. Appl. Phys. [4].

3.2 USSC Microwave-Deposited a-$Si_{1-x}Ge_x$:H

A series of five a-$Si_{1-x}Ge_x$:H alloys was deposited by a microwave plasma technique at USSC with high deposition rates from 1 to 4 nm/s and under different substrate bias conditions [5]. Figure 2 and Table 2 present the results of the SAXS analyses. Ge content and flotation densities are included in the table.

Table 2. SAXS results from series of five microwave-deposited a-$Si_{1-x}Ge_x$:H alloys.

sample # (prep. cond.)	x	ρ(flot) (g/cm^3)	ρ(crys)	t (μm)	Q_N (a)	I_d (e/a)	A (b)	<R> (nm)	$(Q_0/Q_{45})_N$	f_c (%)
2092 (4nm/s, bias off)	0.59	3.89	4.19	3.3	38	64	6	1.6	2.4	4.2
2093 (4nm/s, bias on)	0.54	3.99	4.04	2.2	<0.03	71	8	--	--	<0.01
2193 (2nm/s, bias on)	0.56	3.93	4.10	2.0	27	67	17	1.4	5.2	2.0
2303 (1nm/s, bias on)	0.62	>4.05	4.28	1.4	<0.03	105	22	--	--	<0.01
2304 (1nm/s, bias off)	0.65	4.05	4.36	1.3	58	61	23	1.6	2.9	5.3

a. Units = $10^{24}eu/cm^3$; b. Units = eu/nm^3

Notes: x was determined at NREL by EPMA (Alice Mason); t is the thickness based on x-ray absorption; The subscript N indicates the Q's due only to the nanostructural features without the A/q^3 term [1,2]; f_c is the corrected void volume fraction based on the Q_0/Q_{45} ratio and the ellipsoidal model [1,2].

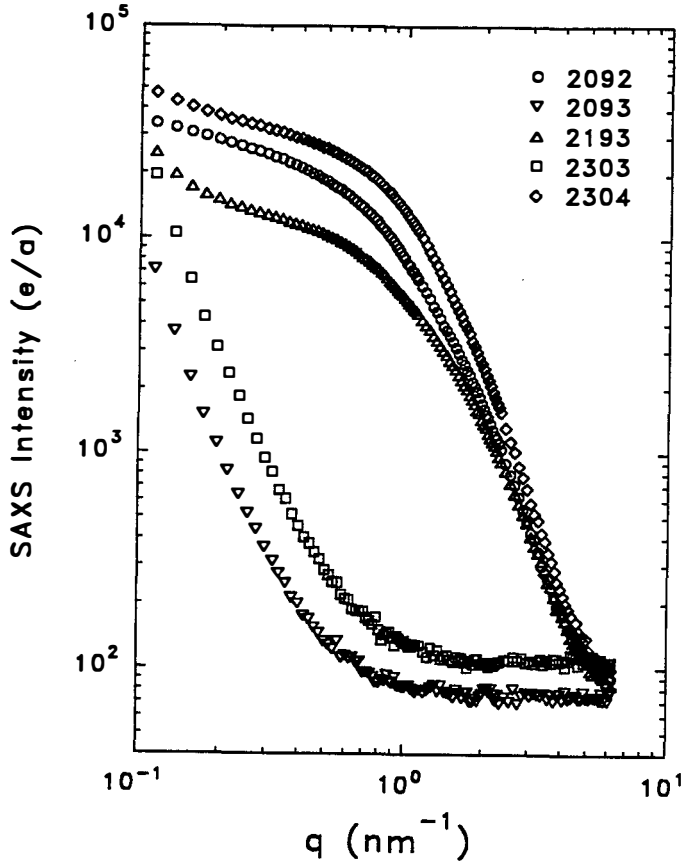

Fig. 2. SAXS intensities from the USSC microwave-deposited a-$Si_{1-x}Ge_x$:H alloys.

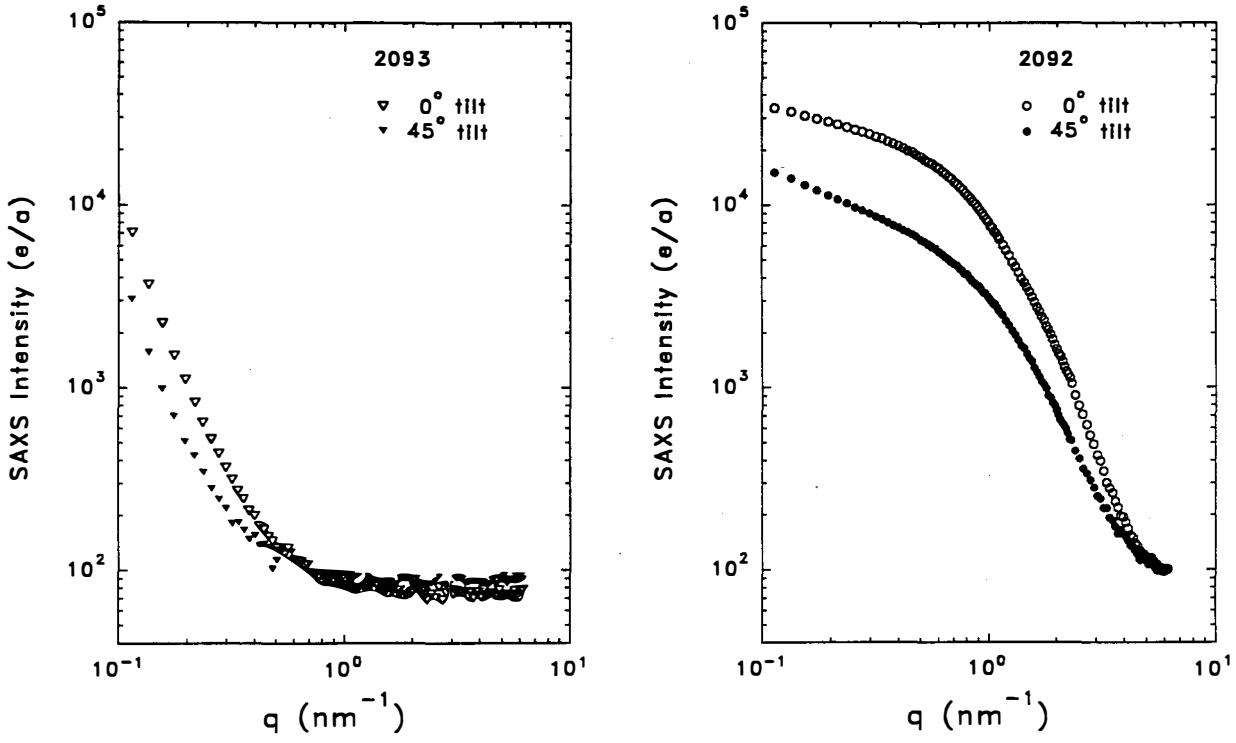

Fig. 3. Effect of sample tilting on the SAXS from two USSC samples.

Standard x-ray diffraction from all 5 samples shows no evidence of any crystallinity. The SAXS data in Fig. 2 and Table 2 show dramatic differences among the samples: 2093 and 2303 show no detectable Q_N, while 2093, 2193, and 2304 show very strong intensities and large Q_N. A noteworthy result is that 2193 does not seem to fit the trend of low SAXS when the bias is on during deposition. Solar cells made with bias on yield the best characteristics [5]. Figure 3 shows the tilt data for two of the samples.

The x values and the flotation densities are nicely consistent. Table 2 includes the densities expected for crystalline alloys. Note that 4.05 g/cm^3 is the highest density we can measure due the limit of our fluid. The estimated void fractions (f_c) are all lower than the density deficits, $1 - \rho(flot)/\rho(crys)$, and this is readily explained by the H alloying effect (and perhaps an average bond-length increase in the amorphous state).

According to the EPMA analyses, samples 2092 and 2304 had quite significant oxygen contamination (4.7 and 14.1 at.%, resp.), consistent with the more porous nanostructure. The other samples were: 2093-1.1%, 2193- 2.3%, 2303- 2.2%. These oxygen contents were not included in the x values (i.e., x was based only on the Si/Ge ratios).

For the two samples with the very weak SAXS (2093, 2303), accurate values for the diffuse intensity, I_d, shows a higher level for 2303. This implies significantly more H in this sample.

The average radii, <R>, are quite small and represent the dimension obtained with the samples untilted. No values could be obtained for two samples due to undetectable Q_N's and the steep rise at low q for these two samples must be due to larger-scale features (R >10 nm) due either to surface roughness or some residual (weak) microstructure. The A's do show some tilt dependence (see, e.g. Fig. 3) such that A_0/A_{45} = ~4 for 2093 and ~10 for 2303.

3.3 IACS He-Diluted a-Si:H

The a-Si group at IACS has developed a technique for fabricating lower bandgap a-Si:H using He dilution during high-pressure PECVD [6]. A series of 5 a-Si:H films prepared with 94% He dilution of a silane plasma and chamber pressures ranging from 0.5 to 2.0 Torr have been analyzed. The properties of the 5 films, the flotation densities, and the SAXS results are summarized in Table 3.

Table 3. Results for IACS Series of He-diluted a-Si:H films.

sample	E_{opt}(Tauc) (eV)	σ(dark) (S/cm)	ημτ (cm^2/V)	ρ(flot) (g/cm^3)	Q_N (eu/cm^3)	A (eu/nm^3)	I_d (eu)
P0	1.675	4.69E-10	1.91E-5	2.234	≤ 2E22	13.5[a]	16
P1	1.59	5.22E-10	1.84E-5	2.240	≤ 2E22	3.5	15
P3	1.54	3.33E-9	9.74E-5	2.226	≤ 2E22	2.5	15
P4	1.50	4.76E-9	5.57E-5	2.231	≤ 2E22	2.0[b]	14
P5	1.60	4.35E-9	2.90E-5	2.219	≤ 2E22	0.7	15

a. $A(0^o)/A(45^o) = 13.5/2$

b. $A(0^o)/A(45^o) = 2.0/0.2$

Figure 4 shows the SAXS data from all five samples. The SAXS intensity is very weak above $q = 1\ nm^{-1}$ and is essentially independent of q in this range, corresponding to only diffuse scattering, I_d. There are steep rises at low q as characterized by the A parameter (coefficient of q^{-3} term), indicating different amounts of some larger-scale microstructure (>20 nm). This larger-scale structure has some orientation since Fig. 5 shows a tilting effect such that A decreases significantly upon tilting to 45 degrees. We are not able to detect any nanostructural SAXS (I_N) so that the integrated intensity due to such features (Q_N) is estimated to be less than $2x10^{22}$ eu/cm^3. The latter value corresponds to 0.01 vol.% nanovoids. Thus this He-diluted, low-gap material is quite homogeneous on this scale but contains a small amount of larger-scale features that seem to be related to residual columnar-like microstructure (in view of the tilting effect). The latter seems to decrease systematically with the number of the series (from P0 to P5).

Note that the flotation density is nearly constant at 2.23 ± 0.01 g/cm^3 for all samples, consistent with no differences in nanovoid fractions among the samples. The density deficit compared to c-Si (2.33 g/cm^3) must be due to the H alloying and the likely bond-length extension in the amorphous state. We also checked all of the samples by conventional x-ray diffraction and found no evidence of microcrystallinity.

USSC made an attempt to reproduce this low-gap material in a device [7] but could not achieve a reduced V_{OC} that would have been consistent with such a lowering of the optical gap indicated in Table 3 (and Ref. 6).

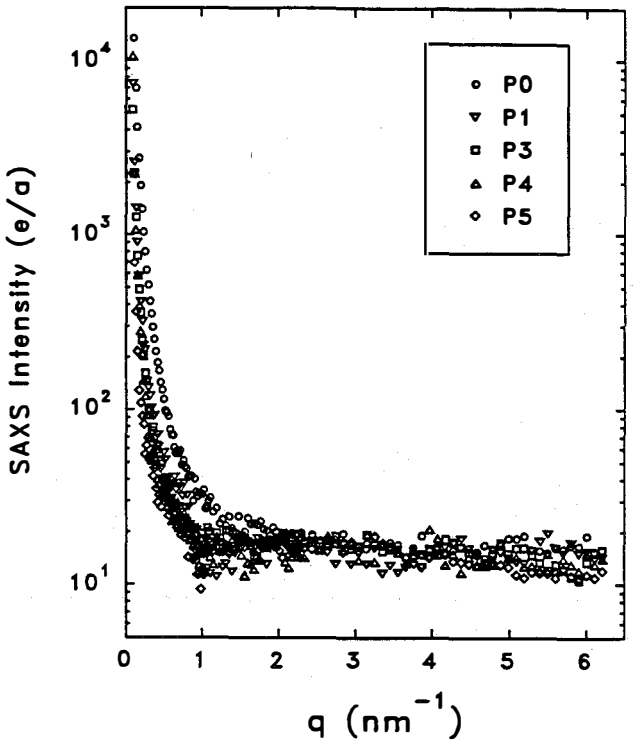

Fig.4. SAXS intensities from IACS He-diluted a-Si:H films.

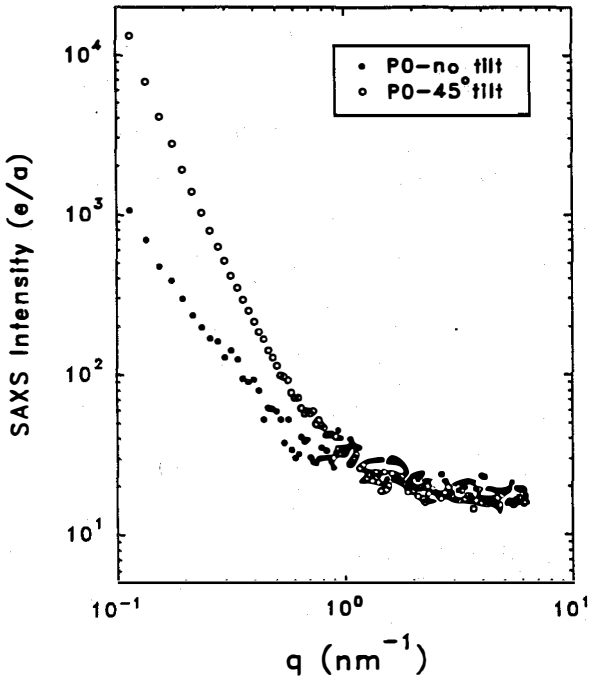

Fig.5. Effect of tilting of sample on SAXS intensity of an IACS He-diluted film.

3.4 ASAXS of a-$Si_{1-x}Ge_x$:H

As noted in an earlier report, several a-$Si_{1-x}Ge_x$:H films previously prepared by several groups (USSC, Harvard, Solarex, Stuttgart, Ecole Polytechnique, and IACS) for SAXS measurements at CSM have been sent to a group at the synchrotron in Hamburg, Germany (DESY). A brief report has been prepared [8] describing initial results from one of the films (IACS#26, x=0.54).

The experiments were carried out at the JUSIFA-beamline in the energy range of the Ge-K-absorption edge between 10.7 and 11.103 keV and with two different orientations (0^o, 45^o) of the sample surface relative to the beam in the same way the tilt measurements are made at CSM. With this technique, SAXS measurements are made near and far from the Ge-K-absorption edge and any difference in intensity is due only to Ge density fluctuations.

In Fig. 6 the two-dimensional scattering patterns of IACS#26 with the two orientations are shown. The 45^o-orientation exhibits a strong anisotropy, which can be associated with columnar-like microstructure previously reported for this film [9]. From the ASAXS-analysis of the vertical and horizontal slices in Fig. 6b obtained at different energies the scattering contributions of the Ge were separated. As can be seen in Fig. 7b, the separated scattering of Ge in the horizontal slice is reduced by an order of magnitude with respect to the vertical slice indicating that the Ge is mainly distributed in columnar-like microstructures. That is, the Ge composition flutuations are mimicing the columnar-like microstructure previously reported [9]. From the separated scattering curve of Fig. 7a, a correlation length of about 7 nm was estimated for the Ge-rich regions.

Thus we have the first direct evidence of non-uniform Ge alloying and the Ge may be clustering along the column boundaries. Further results from several of the other samples will be crucial to decide if IACS#26 is a special case or whether Ge composition fluctuations are a common occurence.

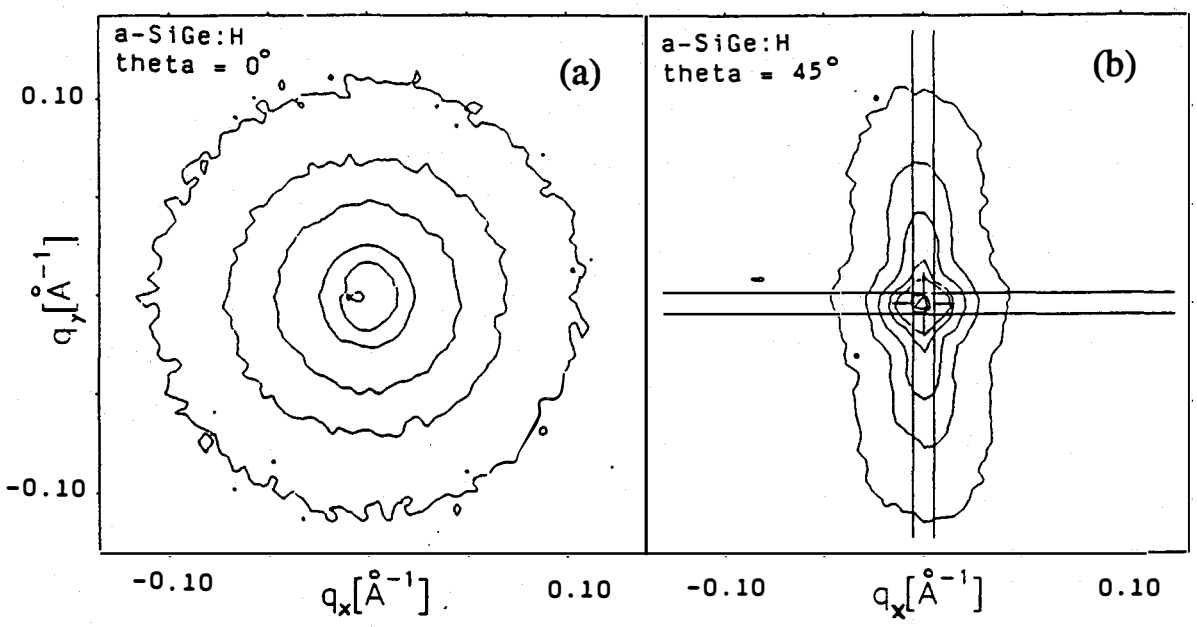

Fig. 6. Two-dimensional scattering patterns of one specimen (I26 x=0.54) at different orientations: (a) 0° and (b) 45°.

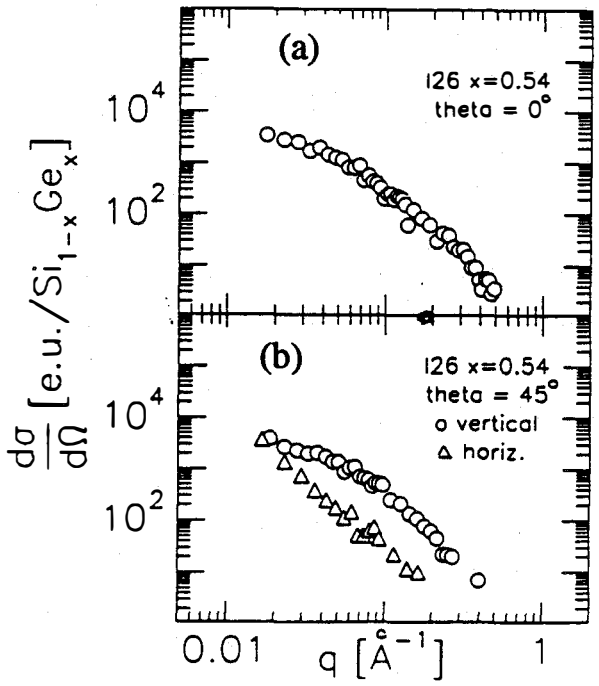

Fig. 7. Separated scattering curves of a-$Si_{1-x}Ge_x$:H with x=0.54 (I26) obtained from the (a) untilted geometry (0°) and the (b) tilted geometry (45°). The two curves in Fig. 7b were obtained from the horizontal and vertical slices of Fig. 6b.

4. MID-BANDGAP MATERIALS

4.1 NREL Hotwire a-Si:H Device Material

The a-Si group at NREL has been experiencing changes in the hotwire a-Si:H film properties as each filament ages so it was decided to compare the nanostructure of a film made at the beginning and near the end of the life of a tungsten filament. The two samples made were THD76 (new filament) and THD79 (old filament) and the conditions used represent those being used to make the solar cells currently under study in the team project between NREL and USSC. Figure 8 shows a comparison of the SAXS from the THD76 film to that from a device-quality PECVD film. Also shown for comparison is the SAXS expected for the presence of 0.1 vol.% naovoids; clearly the void fractions are much less than 0.1% and the analysis gives an upper limit of 0.01% for both films. The lower SAXS signals from the THD76 are due to the lower H content which reduces the diffuse (angle-independent) scattering. The flotation density of THD76 was 2.292 g/cm^3 and represents the highest density of any a-Si:H film measured to date, presumably due to its low H content and lack of any detectable nanovoids.

Figure 9 compares the two hotwire films and one can see a large difference in the SAXS. This was found to be due (at least in part) to partial crystallization of THD79 as shown by standard x-ray diffraction data in Fig. 10 where the diffraction peaks of crystalline Si are labeled. It seemed strange that crystallinity would be connected with the filament life so a review of the depositions was made and it was noted that THD76 and THD79 were not grown under identical conditions. The subtrate temperature was 510^o C (external reading) for THD76 and 525^o C for THD79. Also, the deposition times were 60 and 90 minutes, resp. (yielding similar thicknesses of 2 μm). Thus, apparently the slightly higher temperature and longer deposition time led to partial crystallization of the a-Si:H in THD79. This behavior is not unexpected based on our earlier work demonstrating the Al-induced crystallization of a-Si:H and a-Ge:H associated with the SAXS Al-foil substrates [10]. However, we became concerned about the possibility that the hotwire films may be partially microcrystalline even on glass, Si or the stainless steel substrates being used for the devices. Several hotwire films on glass, Si and stainless steel were supplied by NREL and x-ray diffraction measurements were made on these. No evidence of microcrystallinity was found so the result shown in Fig. 10 is probably due to the a-Si:H/Al-foil interaction although we cannot yet rule out some unusual end-of-life filament effect on the microstructure since this could have been masked by the strong effect of the microcrystals on the SAXS in Fig.9.

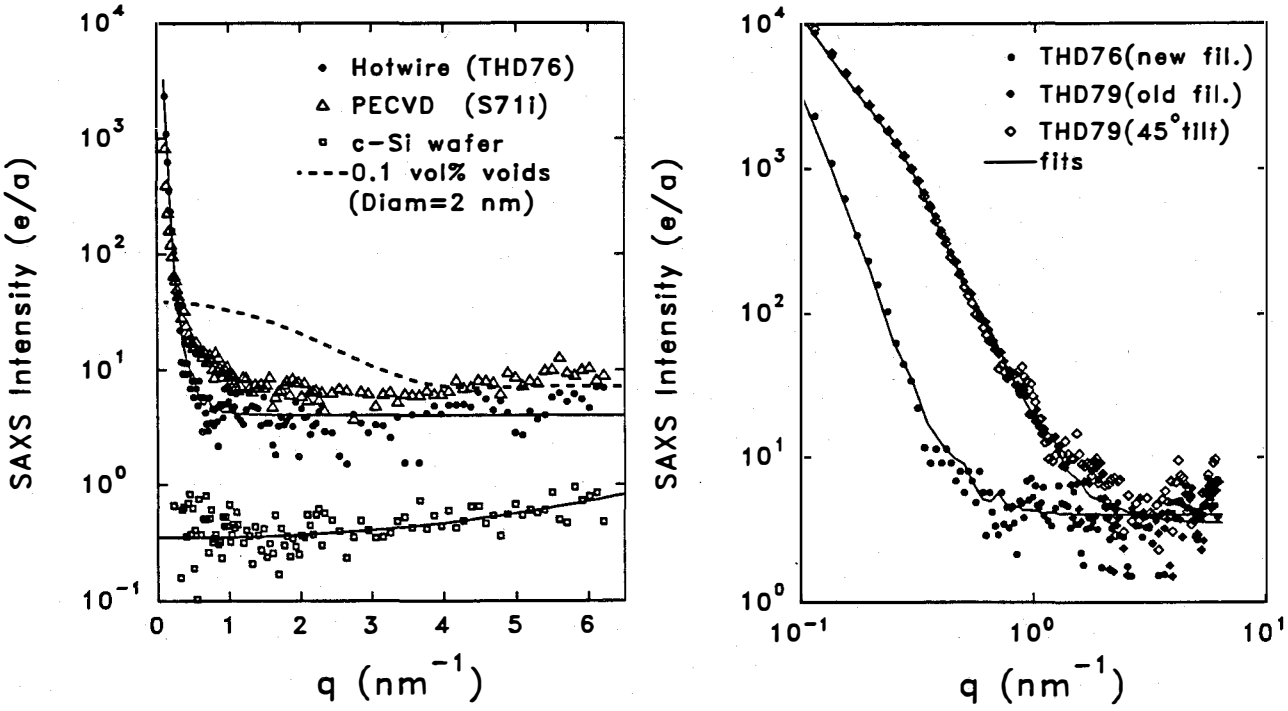

Fig. 8. (left) Comparison of SAXS from current device-quality hotwire a-Si:H and device-quality PECVD a-Si:H. Also shown is expected SAXS from 0.1 vol.% voids.
Fig. 9. (right) SAXS from two hotwire films made at the beginning and near the end of a filament lifetime. Also shown is absence of any tilt effect for sample THD79.

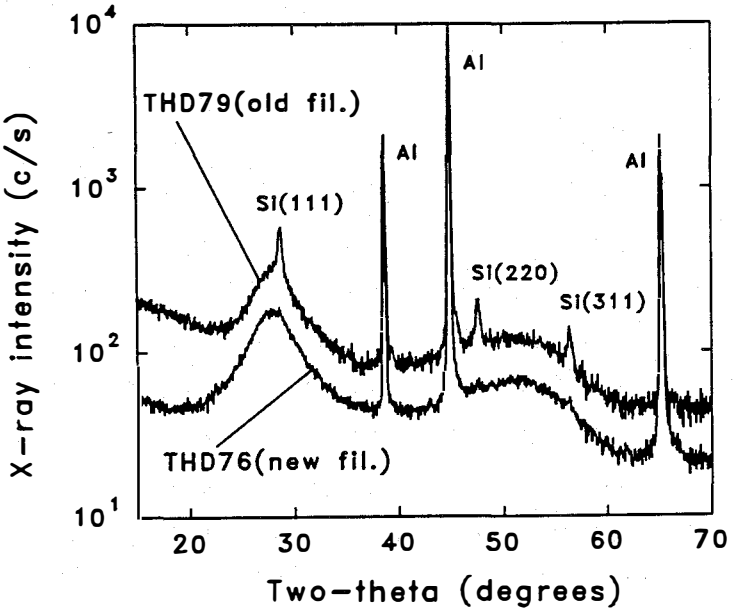

Fig. 10. Comparison of standard x-ray diffraction data from the same two hotwire films studied by SAXS in Fig. 9. Crystalline Si peaks are labeled by their Miller indices.

4.2 ECD a-Si:H High V_{oc} Material

A film of a-Si:H prepared with the same conditions used as an i-layer in single junction cells with initial V_{oc} = 1.04-1.05 V and stabilized V_{oc} = 1.01 V was received for structural characterization. Figure 11 shows the very weak SAXS from the ECD sample. For comparison the expected SAXS from 0.1% voids of average radius 2 nm is shown. The signals from the ECD sample are clearly much less than this. Also, the SAXS at low q shows little or no tilt effect so this larger-scale structure (surface roughness?) has no preferred orientation. Standard x-ray diffraction measurements showed no evidence of microcrystallinity.

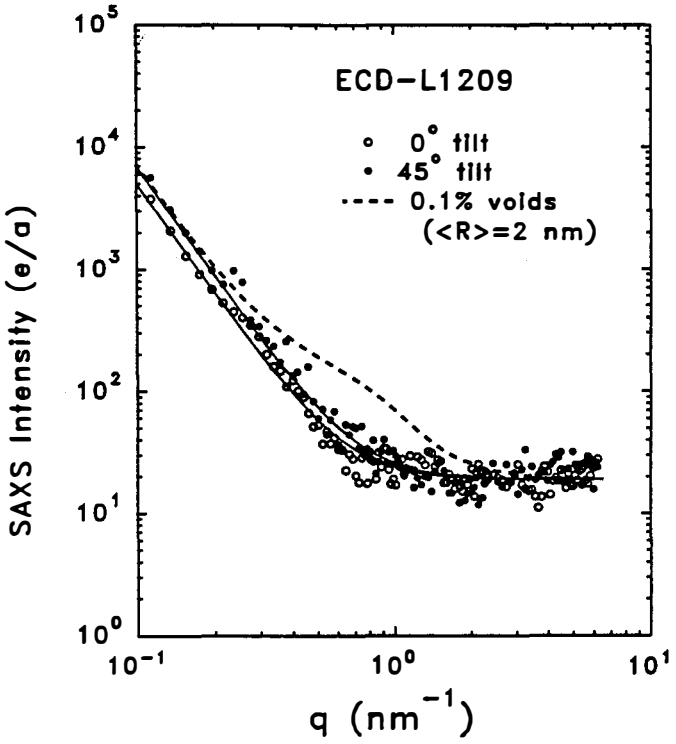

Fig. 11. SAXS from ECD a-Si:H, high V_{oc} material.

The x-ray absorption data yield a film thickness of 0.8 microns. This is thinner than our typical samples and is the cause of the observed scatter in the data. In addition to the SAXS film on Al-foil (L1209), flakes were provided that came loose from films on glass due to poor adhesion and another film on glass (L1204) that was also coming loose from the substrate. Flotation density measurements were made on all three samples with the following results:

L1209 (on Al foil) - 2.166 g/cm^3
L1204 (on glass) - 2.162
flakes in vial - 2.162

Since our uncertainity is about ±0.005 g/cm^3, there is no difference in the film density for the two types of substrates. However, this density is significantly lower that typical device-quality PECVD material (2.22-2.25 g/cm^3). Based on our density data versus H content, the above values are consistent with a total H content of about 18 at.%. This is also consistent with the diffuse scattering level of about 19 e/a which is about twice the level from samples containing 8-10 at.% H (see, e.g.the data from the NREL sample in Fig. 1 of Ref. 2).

4.3 UCB Boron Doping of a-Si:H

The group in the Electrical Engineering Department at UC-Boulder under the direction of G. Moddel prepared four films of a-Si:H with increasing levels of B doping. These were characterized as i, p^{--}, p^{-}, and p^{+} samples. All were deposited at 200°C on 70 μm c-Si substrates with a doping source of 1%TMB in He. Figure 12 shows the systematic increase in SAXS intensities with increased B doping. Duplicate samples were measured for the i and p^{+} samples and the data demonstrate good reproducibility. Note that these data came from a single layer on the c-Si substrates. Assuming the SAXS to be due to spherical nanovoids we find the following diameters and volume fractions from the data in Fig. 12.

Table 4. SAXS results for B-doped a-Si:H films.

Sample	nanovoid diam. (nm)	volume fraction (%)
i	~4	0.04
p^{--}	1.8	0.26
p^{-}	1.2	1.0
p^{+}	1.0	2.1

Note that there is about a 50-fold increase in nanovoid volume fraction induced by the p^{+} level of B doping compared to the intrinsic a-Si:H. The sizes observed are similar to those found in a-SiC:H induced by C alloying [1,2].

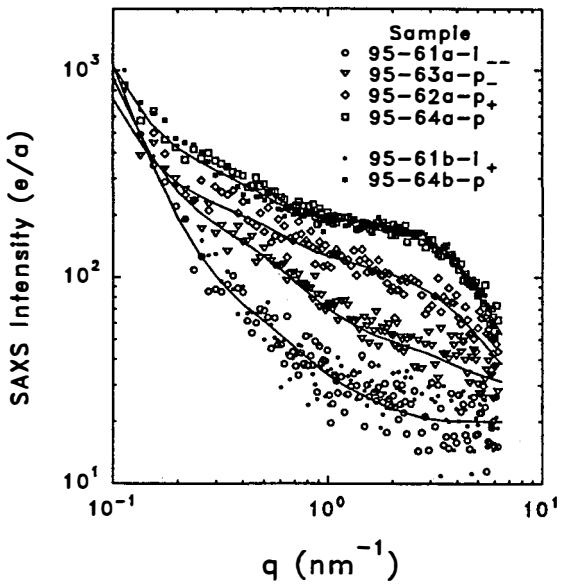

Fig. 12. Effect of B doping of PECVD a-Si:H on the SAXS intensities.

5. HIGH-BANDGAP MATERIALS

5.1 TIT High-Bandgap a-Si:H via Chemical Annealing

Two series of films prepared by the "chemical annealing" method [11,12] at the TIT have been investigated. Five samples were made with various ratios of T1 (time for deposition) and T2 (time for hydrogen-plasma treatment), all at the low substrate temperature of 100°C. The second set of 4 samples was deposited at various substrate temperatures. Defect densities were measured to be less than $10^{16}/cm^3$ and there is evidence of increased stability for this high-gap material [13]. The SAXS samples, deposition conditions, and known properties are listed in Table 5.

Series #1 Analyses

We became suspicious of the strong SAXS signals from some of the samples so we checked for microcrystallinity by x-ray diffraction (XRD) and found three of the films to be at least partially microcrystalline. It was discovered that we could distinguish the microcrystalline areas by a different appearance: grayish versus redish colors - the grayish = microcrystalline (μc) and redish = amorphous (probably due to the higher bandgap of the amorphous areas). This is documented by the XRD patterns in Fig. 13 for the five samples. The sharp peaks are from the Al-foil substrate. We find:

Table 5. Deposition conditions and properties of TIT a-Si:H films.

sample	substrate T (°C)	Dep. rate (nm/s)	Thickness (μm)	T1(s)/T2(s)	Optical gap (eV)	H-content (at.%)
Series # 1						
AR74	100	0.170	2.14	continuous	1.75	12.1
AR76	100	0.184	1.76	10/20	2.01	21.3
AR77	100	0.139	1.39	10/40	2.05	11.1
AR78	100	0.150	1.80	20/40	2.02	22.2
AR79	100	0.180	1.80	10/10	1.91	17.1
Series # 2						
AR173	125	--	1.0	10/10	--	--
AR178	100	--	1.0	10/10	1.92	21.7
AR176	75	--	1.0	10/10	--	--
AR177	50	--	1.0	10/10	1.94	23.9

AR74 - uniform appearance and amorphous.

AR76 - about 50% of area is redish (labeled "r" on Fig. 13) and 50% is grayish (labeled "g" on Fig. 13). The Miller indices of the μc-Si are indicated.

AR77 - uniform appearance and microcrystalline.

AR78 - about 70% of area is redish and about 30% is grayish.

AR79 - uniform appearance and amorphous.

Based on the widths of the μc peaks we estimated the crystallite sizes (L) using the Scherrer equation: for sample AR77 - L(111) = 8.0 nm, L(220) = 4.6 nm, and L(311) = 5.3 nm. (The AR76 and 78 samples look similar in linewidth to AR77).

After discovering the different μc-Si and a-Si:H regions we were careful distinguish which parts of the film were used for the density measurements. Table 6 gives the results which we believe are accurate to ±0.005 g/cm^3.

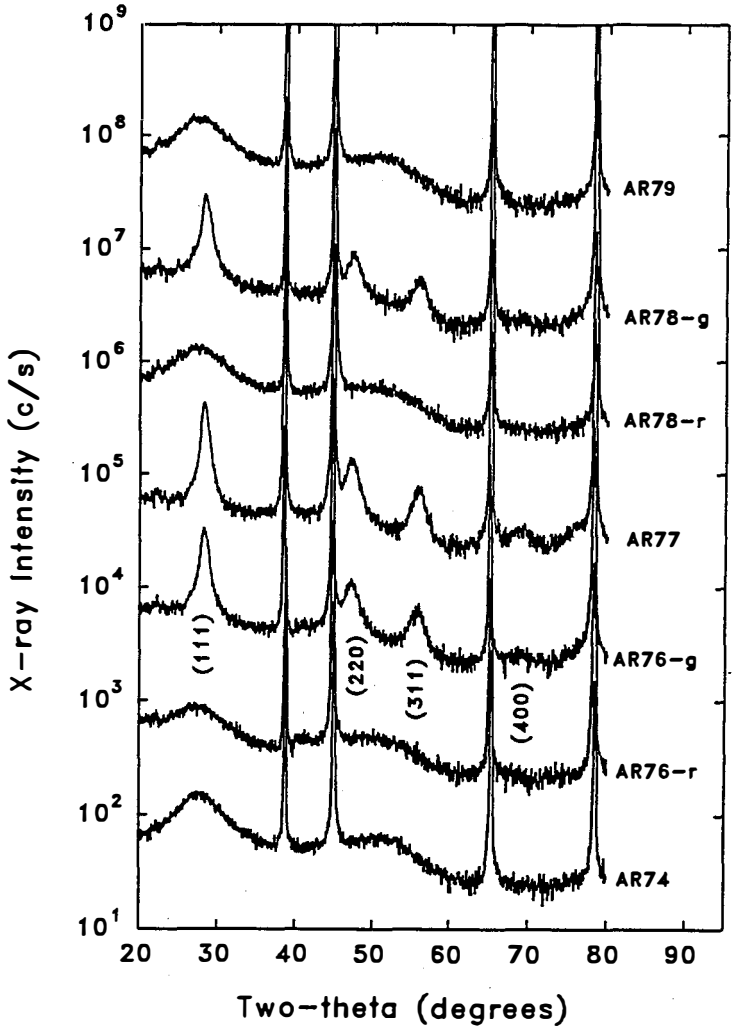

Fig. 13. Standard x-ray diffraction data from TIT series #1 films.

Table 6. Flotation density results for TIT series #1 samples.

Sample	appearance (structure)	density (g/cm^3)
AR74	uniform (a-Si:H)	2.149
AR76-r	redish (a-Si:H)	1.994
AR76-g	grayish (μc-Si)	2.122
AR77	uniform (μc-Si)	2.134
AR78-r	redish (a-Si:H)	1.937
AR78-g*	grayish* (μc-Si)	2.070*
AR79	uniform (a-Si:H)	2.042

(*we think this piece also included some of the redish amorphous phase)

Thus one can see that the μc-Si tends to be more dense although the fully-amorphous AR74 is more dense than any of the samples or regions. Recall that the density of c-Si is 2.33 g/cm^3 so the density deficits range from 17% (AR78-r) to 8% (AR74). As will be seen from the SAXS, such large deficits are mostly due to H alloying.

Since each of the five samples was folded to make 8 layers, the mixed-structure samples (AR76 and AR78) yielded contributions from both μc-Si and a-Si:H. Figure 14 shows the SAXS intensities together with the data from a high-quality PECVD sample made at NREL [Fig. 1 in ref. 2]. The two fully amorphous samples (AR74 and AR79) yielded the weakest SAXS, while the fully microcrystalline sample (AR77) yielded the strongest SAXS. Consistent with these results, the mixed-structure samples yield signals in between. Figure 15 shows the effect of tilting two of the samples by 45^o to look for anisotropic scattering. The observed decreases upon tilting are consistent with elongated scattering objects aligned parallel with the growth direction. The results of the SAXS analyses are provided in Table 7.

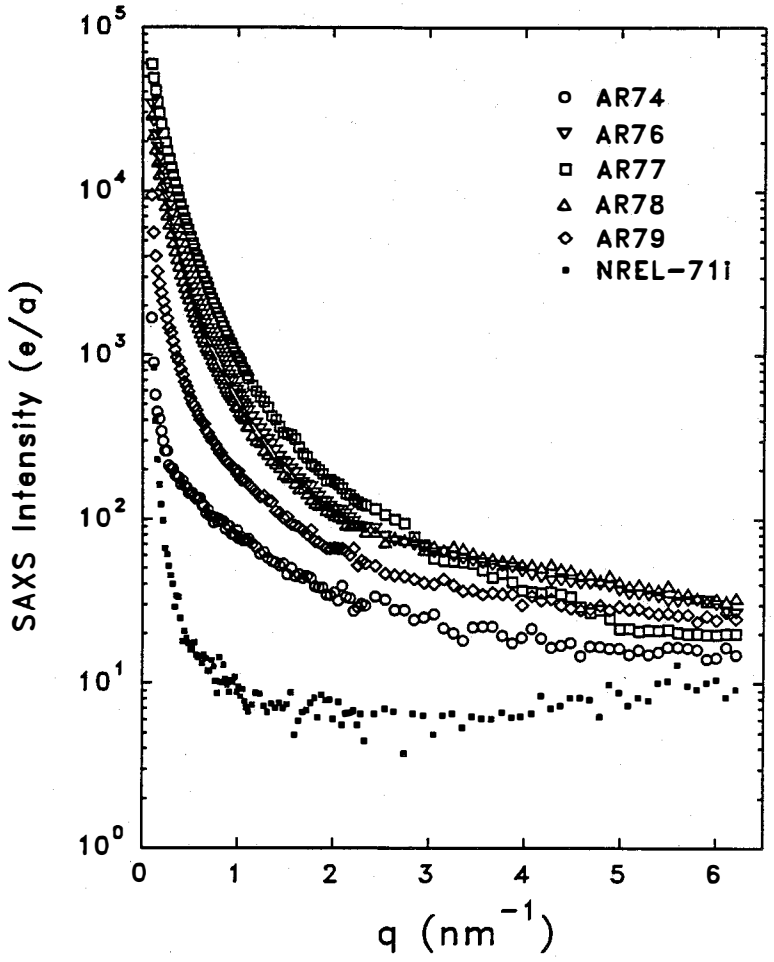

Fig. 14. SAXS from TIT series #1 a-Si:H films and from NREL device-quality film.

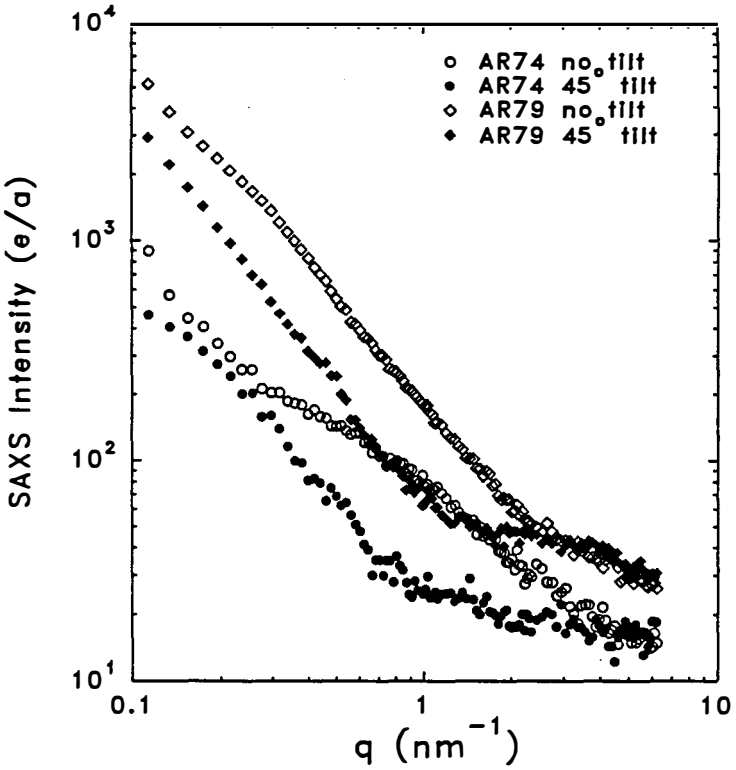

Fig. 15. Effect of sample tilting on SAXS from two TIT a-SI:H series #1 films.

Table 7. SAXS results from TIT series # 1 samples.

sample	Q (eu/cm^3)	A (eu/nm^3)	I_d (eu)	<R>	Q_o/Q_{45}
AR74	4.3E23	1.2	14	1.2	3.1
AR76	4.4E24	22	23	3.3	
AR77	7.5E24	35	12	3.7	
AR78	3.5E24	20	26	3.2	
AR79	1.1E24	6	22	2.3	1.8

As can be seen, the integrated SAXS intensity, Q, is lowest for AR74, about a factor of two larger for AR79, and more than an order of magnitude higher for AR77. The A parameter is a measure of larger-scale microstructure (>20 nm) and seems to scale with Q. The volume-weighted average radius of the scattering objects, <R>, also seems to increase with Q. Note that the average diameter for AR77 is 7.4 nm and this is consistent with the crystallite sizes estimated above from the XRD peak widths. Thus the <R> is most likely related to the μc state for AR76-78, while for AR74 and 79 it is more likely a measure of nanovoid sizes. The tilt ratios Q_o/Q_{45} for AR74 and 79 are both >1, consistent with elongated and oriented nanovoids in a columnar-like structure.

The values of the diffuse scattering intensity, I_d, correlate quite well with the amount of H in the films. This is reasonable since the diffuse scattering from a binary alloy will scale with alloy content [1,2].

We can estimate the maximum possible volume fraction of nanovoids in AR74 and AR79 using Eq.4 of ref. 2 assuming n_p=0 (void) and n_m=n(c-Si)ρ(film)/ρ(c-Si), i.e. the electron density of the matrix is that of c-Si reduced by the ratio of flotation density of each film to the density of c-Si. We say this will be the "maximum possible" because the tilt ratio>1 says the scattering is anisotropic so the experimental Q is larger than the value expected from a sample with randomly-oriented voids. We find:

AR74 f = 0.26 %

AR79 f = 0.75 %

Clearly these values do not account for the measured density deficits, which can be attributed mainly to the H alloying. However, these are quite high void fractions compared to typical device-quality a-Si:H (usually well below 0.1%).

We can also estimate the volume fraction of μc-Si in AR77 assuming n_p=n(c-Si) and n_m= n(c-Si)ρ(a-Si:H)/ρ(c-Si), where ρ(a-Si:H) = [ρ(film)-fρ(c-Si)]/(1-f) and f is the μc volume fraction. We find:

AR77 f =85 %.

We are not sure how reliable this value is since it implies the density of the remaining amorphous fraction is only 1.02 g/cm^3. Anyway, the XRD data in Fig. 13 suggests it is predominantly microcrystalline.

Series #2 Analyses

This series of 4 samples was prepared with various substrate temperatures while other deposition conditions were fixed (Table 5). Figure 16 shows the data and fits for the samples in the untilted orientation. Figure 17 shows the strong effect of tilting one of the samples by 45 degrees. The drop in intensity indicates oriented, non-spherical scattering objects, probably associated with columnar-like growth. Table 8 shows all of the results of the measurements and analyses.

As can be seen from the data in the table, the results are quite systematic:

i) The flotation density decreases with decreasing substrate temperature.

ii) The integrated SAXS intensity (Q) increases with decreasing substrate temperature, corresponding to more scattering features (low-density H-rich regions or nanovoids).

iii) The ratio Q_o/Q_{45} increases with decreasing substrate temperature corresponding to more oriented scattering features.

iv) The average radius <R> (corresponding to the minor axis if ellipsoids assumed with

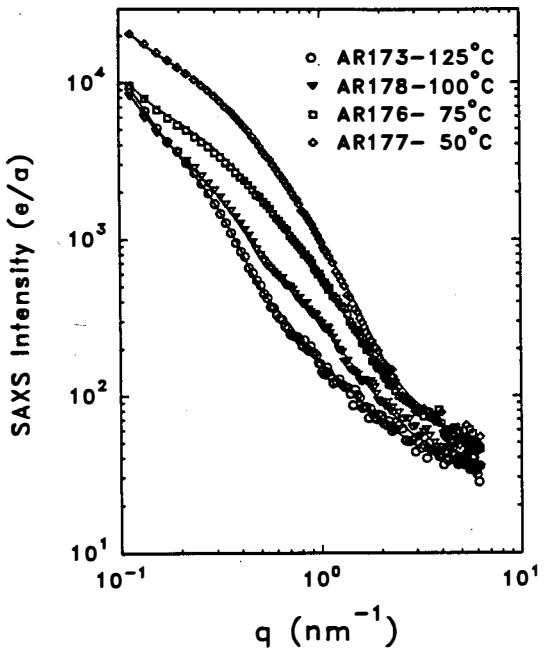

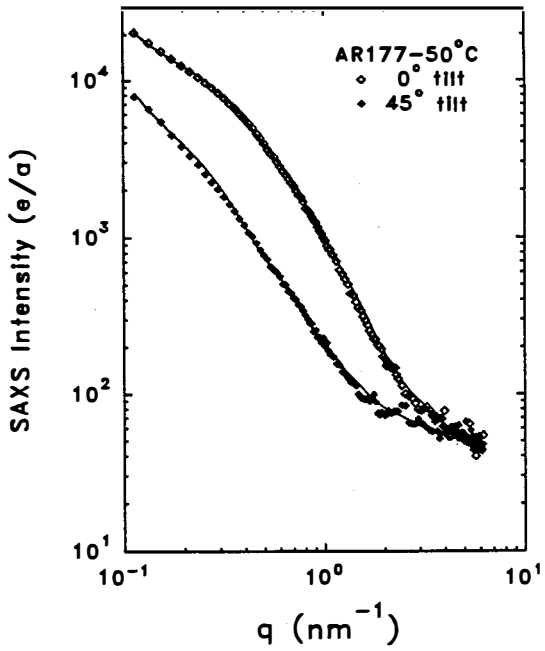

Fig. 16 (left) SAXS data from TIT series #2 films.
Fig. 17. (right) Effect of tilting on SAXS from one of the TIT series #2 films

Table 8. SAXS and flotation density results from TIT series # 2 samples.

Sample	ρ(flot) (g/cm^3)	Q ($10^{24}eu/cm^3$)	A (eu/nm^3)	I_d (eu)	<R> (nm)	Q_o/Q_{45}	f(max) (%)	f(cor) (%)
AR173	2.088	0.99	9	34	2.8	2.2	0.6	0.3
AR178	2.067	1.69	8	33	2.2	3.8	1.0	0.4
AR176	2.020	3.32	6	48	2.3	3.9	1.9	0.7
AR177	2.000	6.15	11	40	2.7	4.8	3.6	1.2

long axes parallel to growth direction) remains between 2.2 and 2.8 nm.

v) If the Q's are converted to void fractions then f(max) represents the maximum possible fraction (assuming zero electron density in the voids) neglecting the tilt effects. f(cor) represents void fractions based on the simple ellipsoidal model with the tilt ratio used to estimate the corrected void fractions.

Note that even the f(max) values are not able to account for the changes in flotation density and this is likely due to the increasing amounts of H incorporated at the lower substrate temperatures (Table 5).

None of these 4 samples showed any evidence of microcrystallinity according to XRD.

Acknowledgements

We thank all the groups who supplied the samples and relevant opto-electronic data for this research. Composition measurements by A. Mason of NREL are gratefully acknowledged.

7. REFERENCES

1. D.L. Williamson, Annual Subcontract Report, NREL/TP-411-8122, August 1995.
2. D.L. Williamson, Mat. Res. Soc. Symp. Proc. **377**, 251 (1995).
3. K.D. Mackenzie, J.R. Eggert, D.J. Leopold, Y.M. Li, S. Lin, and W. Paul, Phys. Rev. B **31**, 2198 (1 985).
4. P. Wickboldt, D. Pang, W. Paul, J.H. Chen, F. Zhong, C.-C. Chen, J.D. Cohen, and D.L. Williamson, J. Appl. Phys. (submitted March, 1996).
5. S. Sugiyama, X. Xu, J. Yang, and S. Guha, Mat. Res. Soc. Symp. (1996-preprint).
6. S. Hazra, A.R. Midya, and S. Ray, J. Appl. Phys. **78**, 581 (1995).
7. S. Guha, Annual Subcontract Report, NREL/TP-411-20205, October 1995.
8. G. Goerigk and D.L. Williamson, Hamburger Synchrotronstrahlungslabor HASYLAB, am Deutschen Elektronen-Synchrotron DESY, Annual Report 1995, p.II-303.
9. A.R. Middya, S. Ray, S.J. Jones, and D.L. Williamson, J.Appl.Phys. **78**, 4966 (1995).
10. S.J. Jones, A.B. Swartzlander-Franz, Y. Chen, and D.L. Williamson, Mat.Res.Soc. Symp. Proc. **297**, 1049 (1993).
11. D. Das, H. Shirai, J. Hanna, and I. Shimizu, Jpn. J. Appl. Phys. **30**, L239 (1991).
12. H. Shirai, T. Ariyoshi, J. Hanna, and I. Shimizu, J. Non-Cryst. Solids **137-138**, 693 (1991).
13. M. Azuma, K. Nakamura, T. Yokoi, K. Yoshino, and I. Shimizu, Mat. Res. Soc. Symp. Proc. **377**, 191 (1995); K. Yoshino, K. Nakamura, and I. Shimizu, preprint.

REPORT DOCUMENTATION PAGE

Form Approved
OMB NO. 0704-0188

1. AGENCY USE ONLY (Leave blank)	2. REPORT DATE	3. REPORT TYPE AND DATES COVERED
	August 1996	Annual Technical Report, 6 April 1995 - 5 April 1996

4. TITLE AND SUBTITLE
Microstructure of Amorphous-Silicon-Based Solar Cell Materials by Small-Angle X-Ray Scattering: Annual Technical Report, 6 April 1995 - 5 April 1996

5. FUNDING NUMBERS
C: XAN-4-13318-04
TA: PV631101

6. AUTHOR(S)
D.L. Williamson

7. PERFORMING ORGANIZATION NAME(S) AND ADDRESS(ES)
Department of Physics
Colorado School of Mines
Golden, Colorado

8. PERFORMING ORGANIZATION REPORT NUMBER

9. SPONSORING/MONITORING AGENCY NAME(S) AND ADDRESS(ES)
National Renewable Energy Laboratory
1617 Cole Blvd.
Golden, CO 80401-3393

10. SPONSORING/MONITORING AGENCY REPORT NUMBER
TP-451-21584
DE96013075

11. SUPPLEMENTARY NOTES
NREL Technical Monitor: B. von Roedern

12a. DISTRIBUTION/AVAILABILITY STATEMENT

12b. DISTRIBUTION CODE
UC-1262

13. ABSTRACT *(Maximum 200 words)*

The general objective of this research is to provide detailed microstructural information on the amorphous-silicon-based, thin-film materials under development for improved multijunction solar cells. Correlation of this microstructure with opto-electronic properties and device performance is an integral part of the research. The experimental technique used is small-angle x-ray scattering, and it provides quantitative microstructural data on microvoid fractions, sizes, shapes, and their preferred orientations. Other microstructural features such as alloy segregation, hydrogen-rich clusters, and alloy short-range order are probed. Three types of material are under investigation and fall into the bandgap classification scheme forming the basis of three of the four NREL Amorphous Silicon Teams.

14. SUBJECT TERMS
photovoltaics ; amorphous silicon solar cells ; thin-film materials ; small-angle x-ray scattering ; microstructure ; multijunction cells

15. NUMBER OF PAGES
29

16. PRICE CODE

17. SECURITY CLASSIFICATION OF REPORT	18. SECURITY CLASSIFICATION OF THIS PAGE	19. SECURITY CLASSIFICATION OF ABSTRACT	20. LIMITATION OF ABSTRACT
Unclassified	Unclassified	Unclassified	UL